Design and construction of a velocity map imaging spectrometer

Master's thesis
by
Sara Thorin

Lund Reports on Atomic Physics, LRAP-327
Lund, August 2004

Abstract

Spectrometers for measuring electron energies can be useful in many areas in physics . In the Atomic Physics department in Lund an electron spectrometer is used for characterization of attosecond pulses.

The object of this Master's thesis was to design and construct a velocity-map imaging spectrometer which apart from electron energies also give information about the electrons angular distribution. This spectrometer will be used in the attosecond pulse research.

A detailed theory for the differential cross section and angular distribution in photoionization is presented. Simulations of electron trajectories in an electric field has been made and the dimensions of the spectrometer has been designed accordingly along with suitable voltage settings for the electric field and from this an entire imaging setup has been constructed.

Contents

Chapter 1

Introduction

People have always strived to better understand the world around them by looking at it, examining and experimenting. When it comes to understanding very small particles, like electrons, it turns out they are quite difficult to examine.

One way of understanding more about the physics of an electron is knocking it out from its atom and finding out where it goes and what energy it has. Looking in to this process gives information not only on the behavior of the electron, but also on the force that knocks it out from the atom. This means that being able to detect and extract information about the emitted electron would be interesting both from a fundamental physics point of view and for examining physical phenomena that can ionize atoms, for instance lasers, x-rays, particle radiation and collisions. In this thesis it is electrons ionized by laser that will be treated.

An electron can be detected for example by letting it hit a surface where it knocks out several more electrons. These electrons will in their turn hit another surface where they will be multiplied again and so on until a measurable current has been created. This gives a way of detecting if and when an electron has hit a surface, but it does not give any information on the energy of the electron. For this purpose an electron spectrometer is needed.

Electron spectrometers are an important tool in both atomic and nuclear physics as well as in chemistry and biology.

1.1 Electron spectrometers

There exists a number of different ways to measure electron energies. A few examples are the Hemispherical Analyzer, the Time-Of-Flight Spectrometer and the Velocity Map Imaging Spectrometer.

1.1.1 Hemispherical Analyzer

This spectrometer consists of two concentric hemispheres held at different potentials. The electrons enter and leave trough narrow slits. Only the electrons with the right kinetic energy can pass the analyzer at a certain potential difference. If the electrons are traveling very fast they will hit the outer hemisphere and if their kinetic energy is very low they will be attracted to the inner hemisphere. Thus only electrons of a very narrow energy region will be able to pass through the whole analyzer to the detector.

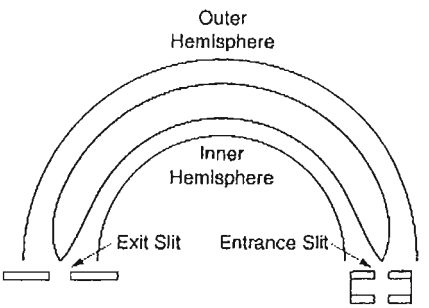

Figure 1.1: Hemispherical analyzer

1.1.2 The Time-Of-Flight Spectrometer (TOF)

A TOF spectrometer is a long tube with a detector on one end. In the other end there are two electrodes with different potentials. Electrons are emitted in the ionization region and will fly toward the detector trough a hole in the inner electrode (see figure 1.2). How long it takes for the the electrons to reach the detector depend on their kinetic energy. By looking at the time of flight with for example an oscilloscope the energy of the electrons can be determined.

One type of TOF spectrometer is The Magnetic Bottle Electron Spectrometer (MBES). In an MBES a magnetic field is created around the TOF tube and the ionization region in the shape of a bottle — hence the name — and the electrons are adiabatically accelerated toward the detector. The MBES is able to collect all electrons with a velocity component towards the detector which give a very high detection efficiency and a much stronger signal compared to the plain TOF.

1.1.3 The Velocity Map Imaging Spectrometer (VMIS)

The development of detectors that can register the position where the electron hit, and the use of CCD-cameras gave rise to a new technique in electron spectrometry called "velocity-map imaging". This technique has been used since 1997 [1].

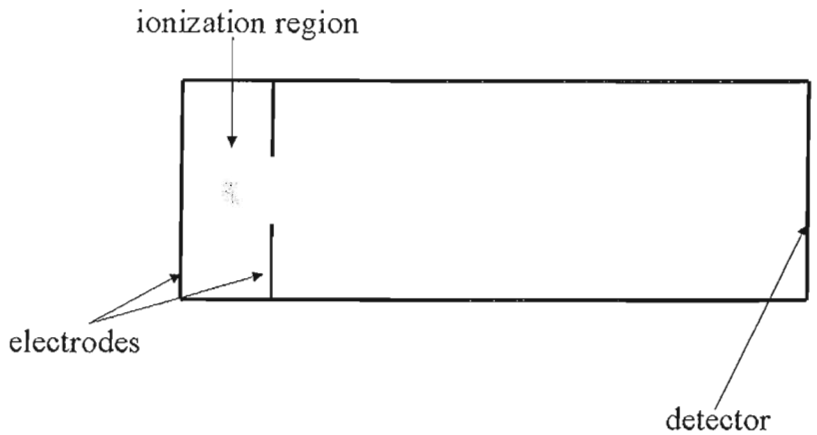

Figure 1.2: Schematic view of time-of-flight spectrometer

The VMIS consists of a long tube with the ionization region in one end and a detector system in the other. On each side of the ionization region there is an electrode with high voltage which creates an electric field, similar to the TOF spectrometer. But in this case the voltages on the two electrodes are so high so that the electrons initial kinetic energy can be neglected in the time-of-flight to the detector. Instead it is the position where the electrons hit the detector, a multichannel plate and a CCD-camera, which give information on the electron energies.

1.2 Motivation for the VMIS

In the Atomic Physics department in LTH, research is being done on high harmonics created by focusing a femtosecond IR laser in a gas. The wavelength of the harmonics extend up to the extreme ultra violet (XUV) region. Harmonics are used to create attosecond pulses or pulse trains [3].

One tool used in analyzing these pulses is an electron spectrometer where the harmonics ionize the detection gas in the spectrometer and the electron energy plus the ionization energy give the energy of the individual harmonics. The atoms in the detection gas can be ionized not only by a single harmonic but also in a two photon process by a harmonic and an initial IR photon. This give rise to sidebands in the electron spectra with energies between two consecutive harmonics. These measurements are done with a magnetic bottle spectrometer described above.

So, why does one want to build a velocity map imaging spectrometer? The difference between the MBES and the VMIS is that the imaging machine gives an actual image of the electrons velocity distribution. If the electrons are emitted from an s-orbital this angular distribution is equal in all directions but if the ionized level is a p-orbital or higher there will be a higher probability for the

electrons to be emitted in certain angles — the differential cross section for photo ionization is angle dependent.

Angular information can be extracted in both TOF and hemispherical spectrometry by either moving the spectrometer in different angles or by changing the polarization of the laser. In the MBES however the angular information is lost due to the fact that the magnetic field redirects the electrons towards the detector. The advantage of the VMIS compared to the TOF spectrometer and the hemispherical analyzer is that all angular information is gathered in one image and nothing needs to be moved or turned.

The angular information given by imaging spectrometry is interesting both from a general scientific point of view, and for a number of applications. The angular distribution of emitted electrons will for example differ for different elements and compounds, different ionized orbitals, number of photons involved in the transition and which electric or magnetic order of the transition (dipole, quadrupole etc.).

In the case of characterizing attosecond pulses it turns out that for single pulses and very short pulse trains the photoelectrons created by single and two photon — IR + harmonic -- ionization overlap in energy. Thus an electron spectrometer just measuring energy would not be able to distinguish between the harmonic and the sideband. But since the angular distribution of photo electrons is different in these two cases an image of the emitted electrons can be used for the analysis [2].

So besides being a way of getting an informative and visual view of the electrons energy spectra, the velocity map imaging spectrometer is an essential tool when the attosecond pulse trains get shorter and shorter and single pulses can be achieved.

Designing and constructing a velocity map imaging spectrometer is the objective of this diploma thesis.

1.3 Outline

This report deals with a wide range of aspects in creating a velocity-map imaging spectrometer. Some are only mentioned briefly while others are discussed in some detail.

Chapter 2 gives a derivation and demonstration of the differential cross section for electrons in photoionization.

The principle of the spectrometer and of velocity-map imaging in general is discussed in chapter 3.

Chapter 4 deals with the design of the VMIS and gives a short explanation of the different constituents.

Chapter 5 includes some measurements done on an imaging machine in Amsterdam, a planned test, and a short manual on how to operate the spectrometer.

Chapter 2

Angular distribution in photoionization

When an atom absorbs electromagnetic radiation it will make a transition to a higher lying state. If the energy is high enough the final state for the electron is in the continuum, that is, the electron is ejected from the atom. This is called the photoelectric effect. In this chapter I will derive the differential cross section for photoionization – which gives the probability for the electron to be emitted in a certain angle – for both one and two photon processes.

2.1 Transition Rates

The time-dependent Schrödinger equation can be written as

$$i\hbar\frac{\partial\Psi}{\partial t} = (\mathbf{H}_0 + \mathbf{H}'(t))\Psi \tag{2.1}$$

where

$$\mathbf{H}_0 = -\frac{\hbar^2}{2m}\nabla^2 - \frac{Ze^2}{4\pi\varepsilon_0 r}$$

is the Hamiltonian describing the one electron atom and

$$\mathbf{H}'(t) = -\frac{i\hbar e}{m}\mathbf{A}\cdot\nabla \tag{2.2}$$

is the time dependent Hamiltonian describing the perturbation, due to the outer electrical field caused by the laser [4].

A is a vector potential that generates the electric field and can for a plane wave be expressed as

$$\mathbf{A}(\vec{r},t) = A_0\hat{\varepsilon}\left(e^{i(\vec{k}\vec{r}-\omega t)} + e^{-i(\vec{k}\vec{r}-\omega t)}\right) \tag{2.3}$$

The unit vector $\hat{\varepsilon}$ is the polarization vector of the laser light.

The interaction between the electrical field and the atom can be treated with time-dependent perturbation theory. The time independent Schrödinger equation for the H_0 Hamilton operator is given by

$$\mathbf{H}_0\psi_k = E_k\psi_k$$

The eigenfunctions ψ_k are normalized wave functions forming a complete set of base functions. We look for a solution to the time-dependent Schrödinger equation of the form

$$\Psi = \sum_k c_k(t)\psi_k(\mathbf{r})e^{-iE_kt/\hbar} \tag{2.4}$$

$|c_k|^2$ describes the probability that the system is in state k at time t.

If it is now assumed that there is no perturbation at time $t = 0$ so that the system at this time is in an eigenstate of H_0, then $c_i(t_0) = 1$ and $c_k(t_0) = 0$ for $k \neq i$, where i stands for *initial*, and the time dependent perturbation theory can be used. The coefficient describing the population in the final state f after interaction with the laser beam is given by

$$c_f(t) = -\frac{i}{\hbar}\int_0^t < \psi_f(\mathbf{r})|\mathbf{H}'(t')|\psi_i(\mathbf{r}) > e^{i\omega_{fi}t'}dt'$$

for the case of one photon ionization. Here ω_{fi} is the frequency difference between the final and initial states. For the two-quantum photoelectric effect the second order perturbation theory is used:

$$c_f^{(2)}(t) = \frac{1}{\hbar^2}\sum_s \int_0^t < \psi_f(\mathbf{r})|\mathbf{H}'(t')|\psi_s(\mathbf{r}) > e^{i\omega_{fs}t'}dt' \int_0^{t'} < \psi_s(\mathbf{r})|\mathbf{H}'(t'')|\psi_i(\mathbf{r}) > e^{i\omega_{si}t''}dt''$$

Using equation (2.2) and (2.3) we obtain in the one photon case:

$$\begin{aligned} c_f(t) &= -\frac{e}{m}A_0\left(\underbrace{< f|\hat{\varepsilon}\vec{\nabla}e^{i\vec{k}\vec{r}}|i >}_{M_{fi}}\int_0^t e^{i(\omega_{fi}-\omega)t'}dt' + \underbrace{< f|\hat{\varepsilon}\vec{\nabla}e^{-i\vec{k}\vec{r}}|i >}_{M_{fi}^*}\int_0^t e^{i(\omega_{fi}+\omega)t'}dt'\right) \\ c_f(t) &= -\frac{e}{m}A_0\left(M_{fi}\left[\frac{e^{i(\omega_{fi}-\omega)t'}}{i(\omega_{fi}-\omega)}\right]_0^t + M_{fi}^*\left[\frac{e^{i(\omega_{fi}+\omega)t'}}{i(\omega_{fi}+\omega)}\right]_0^t\right) \end{aligned} \tag{2.5}$$

If $\omega_{fi} \approx \omega$ the first part of this expression is dominating and the second part can be neglected. This means that a photon is absorbed by the atom and the expression for c_f becomes:

$$\begin{aligned} c_f(t) &= -\frac{e}{m}A_0M_{fi}\frac{e^{i(\omega_{fi}-\omega)t}-1}{i(\omega_{fi}-\omega)} \\ \Rightarrow |c_f(t)|^2 &= 2\frac{e^2}{m^2}A_0^2|M_{fi}|^2\underbrace{\frac{1-\cos(\omega_{fi}-\omega)t}{(\omega_{fi}-\omega)^2}}_{F(t,\omega_{fi}-\omega)} \end{aligned}$$

As $t \to \infty$ it can be shown that $F(t, \omega_{fi} - \omega)$ approaches the value $\pi t \delta(\omega_{fi} - \omega)$ and so

$$|c_f(t)|^2 = 2\frac{e^2}{m^2} A_0^2 |M_{fi}|^2 \pi t \delta(\omega_{fi} - \omega)$$

This is the probability for the system to be in state f at time t if t is large.

The absorption or transition rate is now defined as

$$\frac{d}{dt}|c_f(t)|^2 = W_{fi} = 2\frac{e^2}{m^2} A_0^2 |M_{fi}|^2 \pi \delta(\omega_{fi} - \omega)$$

W_{fi} can be written as a function of intensity per unit angular frequency range, $I(\omega) = 2c\varepsilon_0 \omega^2 A_0^2$.

$$W_{fi} = \pi \frac{e^2}{m^2} \frac{I(\omega_{fi})}{\omega_{fi}^2 \varepsilon_0 c} |M_{fi}|^2 \delta(\omega_{fi} - \omega)$$

The absorption cross section is defined as the rate of absorption of energy divided by $I(\omega_{fi})$, that is,

$$\sigma_{fi} = \frac{\hbar \omega_{fi} W_{fi}}{I(\omega_{fi})} = \frac{4\pi^2 \hbar^2}{m^2 \omega_{fi}} \underbrace{\left(\frac{e^2}{4\pi\varepsilon_0 \hbar c}\right)}_{\alpha} |M_{fi}|^2 \delta(\omega_{fi} - \omega)$$

It is now possible to derive a cross section for a particular photo ionization process. The total cross section is obtained by integrating over the continuous final states of the emitted electron.

$$\sigma_{tot} = \frac{4\pi^2 \hbar^2 \alpha}{m^2} \int d\mathbf{k_f} \frac{1}{\omega_{fi}} |M_{fi}|^2 \delta(\omega_{fi} - \omega)$$

The integration element can be written $d\mathbf{k_f} = k_f^2 dk_f d\Omega$. Using this and the fact that the kinetic energy in the final state is given by $E_f = \frac{\hbar^2 k_f^2}{2m}$, the total cross section can be rewritten as

$$\sigma_{tot} = \frac{4\pi^2 \alpha}{m} \int_0^\infty dE_f \int d\Omega \frac{k_f}{\omega_{fi}} |M_{fi}|^2 \delta(\omega_{fi} - \omega)$$

Performing the integration over E_f with the help of the Dirac function gives

$$\sigma_{tot} = \frac{4\pi^2 \alpha \hbar}{m} \frac{k_f}{\omega} \int |M_{fi}|^2 d\Omega$$

which now leads to the expression for the differential cross section

$$\frac{d\sigma}{d\Omega} = \frac{4\pi^2 \alpha \hbar}{m} \frac{k_f}{\omega} |M_{fi}|^2$$

This gives the probability for the electron to be emitted within the solid angle $d\Omega$ in the direction (θ, ϕ).

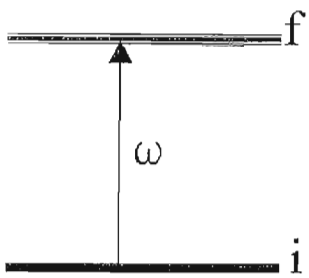

Figure 2.1: Ionization with one photon

In the two photon case the expression for the differential cross section is the same, but the matrix element M_{fi} is a bit more complicated.

$$M_{fi}^{(2)} = \sum_s \frac{< f|\hat{\varepsilon}\vec{\nabla}e^{i\vec{k}\vec{r}}|s >< s|\hat{\varepsilon}\vec{\nabla}e^{i\vec{k}\vec{r}}|i >}{E_i - E_s + \hbar\omega_1 + i0}$$

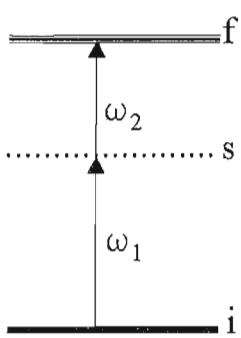

Figure 2.2: Ionization with two photons

In order to calculate cross sections for different transitions the matrix element $|M_{fi}(\omega)|$ has to be evaluated. To make this easier a dipole approximation can be made.

2.2 The Dipole Approximation

This derivation is done for the one photon matrix element, but the procedure is similar in the two photon case.

The exponential in the matrix element $|M_{fi}(\omega)|$, $e^{i\mathbf{k}\cdot\mathbf{r}}$ can be expanded as

$$e^{i\mathbf{k}\cdot\mathbf{r}} = 1 + (i\mathbf{k}\cdot\mathbf{r}) + \frac{1}{2!}(i\mathbf{k}\cdot\mathbf{r})^2 + ...$$

The first term in this expansion correspond to electric dipole transitions. The higher terms represent magnetic dipole, electric quadrupole transitions and so on.

The extent of atomic wave functions is of the order of the Bohr radius of the atom, that is about 1Å. The wave number $k = 2\pi/\lambda$ is for optical transitions of the order 10^3Å. This means that the quantity $\mathbf{k} \cdot \mathbf{r}$ is of the order 10^{-7}m, and $e^{i\mathbf{k}\cdot\mathbf{r}}$ can be approximated with unity. This leads to the electric dipole approximation.

$$M_{fi} =< f|e^{i\mathbf{k}\cdot\mathbf{r}}\hat{\varepsilon}\vec{\nabla}|i >\approx \hat{\varepsilon} < f|\vec{\nabla}|i >$$

Furthermore this expression can be rewritten according to the following calculations:

$$\begin{aligned} \mathbf{p} &= -i\hbar\vec{\nabla} \\ \frac{d}{dt}\mathbf{r} &= \frac{1}{m}\mathbf{p} \\ \Rightarrow M_{fi} &= \hat{\varepsilon}\frac{im}{\hbar} < f|\dot{\mathbf{r}}|i > \end{aligned}$$

The general relation $\frac{d}{dt} < \mathbf{A} >= \frac{i}{\hbar} < [\mathbf{H}, \mathbf{A}] >$ in this case leads to

$$\begin{aligned} < f|\dot{\mathbf{r}}|i > &= \frac{1}{i\hbar} < f|\mathbf{rH} - \mathbf{Hr}|i > \\ &= \frac{1}{i\hbar} < f|\mathbf{r}|\mathbf{H}i > -\frac{1}{i\hbar} < \mathbf{H}f|\mathbf{r}|i > \\ &\approx \frac{1}{i\hbar}E_i < f|\mathbf{r}|i > -\frac{1}{i\hbar}E_f < f|\mathbf{r}|i > \\ &= \frac{1}{i\hbar}\underbrace{(E_i - E_f)}_{-\hbar\omega_{fi}}\underbrace{< f|\mathbf{r}|i >}_{\mathbf{r}_{fi}} \\ &= i\omega_{fi}\mathbf{r}_{fi} \end{aligned}$$

The matrix element M_{fi} finally takes the form

$$M_{fi} = -\frac{m\omega_{fi}}{\hbar}\hat{\varepsilon} \cdot \mathbf{r}_{fi} \tag{2.6}$$

This expression represents the component of the dipole moment in the $\hat{\varepsilon}$ direction between the initial and final states. If (2.6) is non vanishing, the transition is allowed.

2.3 The Differential Cross Section

There are several papers[6][7][9][10] and theses[11] which treat different parts of the angular distribution in the atomic photoeffect. In this section I will demonstrate the major steps in the derivation of the photoionization differential cross section both in the one and two photon case.

2.3.1 One Photon Ionization

The differential cross section in the dipole approximation can now be written as

$$\frac{d\sigma}{d\Omega} = \frac{4\pi^2 \alpha k_f m}{\hbar} \omega |\hat{\varepsilon} \cdot \mathbf{r}_{fi}|^2$$

If it is now assumed that the polarization of the laser is along the z-axis the differential cross section can be written

$$\frac{d\sigma}{d\Omega} = \frac{4\pi^2 \alpha m k_f}{\hbar} \omega | < \Psi_f | \mathbf{z} | \Psi_i > |^2 \tag{2.7}$$

This expression is valid in a one electron system but can be expanded to apply to many electron systems by replacing the z operator by a sum over all electrons.

The wave functions for the initial state and the continuum final state can be written

$$\Psi_i = P_{nl}(r) Y_{lm}(\theta, \phi) \tag{2.8}$$

$$\Psi_f = 4\pi \sum_{L=0}^{\infty} (-i)^L e^{i\delta_L} P_{kL}(r) \sum_{M=-L}^{L} Y_{LM}(\theta, \phi) Y^*_{LM}(\theta', \phi') \tag{2.9}$$

where i symbolizes the the quantum numbers nlm and f symbolizes kLM, k is the momentum of the ejected electron.

z as an operator can be written

$$\mathbf{z} = r \cos\theta = \sqrt{\frac{4\pi}{3}} r Y_{10}(\theta, \phi) \tag{2.10}$$

Using (2.8), (2.9) and (2.10) the matrix element M_{fi} can be calculated

$$M_{fi} \propto 4\pi \sum_{L=0}^{\infty} (-i)^L e^{i\delta_L} R_{nlkL} \sum_{M=-L}^{L} \sqrt{\frac{4\pi}{3}} Y_{LM}(\theta', \phi') < Y_{LM} | Y_{10} | Y_{lm} >$$

where R_{nlkL} denotes the radial integral $\int r P_{nl}(r) P_{kl}(r) dr$.

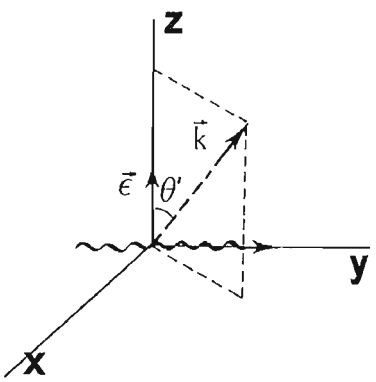

Figure 2.3: Coordinate system showing the angle between the laser polarization and the direction of the the ejected electron.

In the dipole approximation the allowed transitions are $L = l \pm 1$ and $\Delta m = 0$ for linearly polarized light and the sum over M reduces to $M = m$. Now $< Y_{LM}|Y_{10}|Y_{lm} >$ can be calculated.

$$\begin{aligned}
\sqrt{\frac{4\pi}{3}} < Y_{LM}|Y_{10}|Y_{lm} > &= \sqrt{\frac{4\pi}{3}} \int Y^*_{L-m}(\theta,\phi) Y_{10}(\theta,\phi) Y_{lm}(\theta,\phi) d\Omega \\
&= \sqrt{\frac{4\pi}{3}} (-1)^m \left[\frac{(2L+1)(3)}{4\pi(2l+1)}\right]^{1/2} < L100|l0 >< L1m0|lm > \\
&= (-1)^m \left[\frac{(2L+1)}{(2l+1)}\right]^{1/2} < L100|l0 >< L1m0|lm > \qquad (2.11)
\end{aligned}$$

where $< L100|l0 >< L1m0|lm >$ are Clebsch Gordan coefficients.

The sum over L in M_{fi} reduces to

$$M_{fi} = M_{fi}^{L=l-1} + M_{fi}^{L=l+1}$$

The differential cross section is proportional to the square of M_{fi} and summing over all initial states gives the following expression

$$\begin{aligned}
\frac{d\sigma}{d\Omega} &\propto \sum_m |M_{fi}|^2 = \sum_m |M_{fi}^{L=l-1} + M_{fi}^{L=l+1}|^2 \\
&= (4\pi)^2 \sum_m \Bigg[|R_{nlk(l-1)}|^2 \frac{4\pi}{3} \frac{(2l-1)}{(2l+1)} \qquad (2.12) \\
&\quad | < (l-1)100|l0 > |^2 | < (l-1)1m0|lm > |^2 |Y_{(l-1)m}(\theta',\phi')|^2 \\
&+ |R_{nlk(l+1)}|^2 \frac{4\pi}{3} \frac{(2l+3)}{(2l+1)} \qquad (2.13) \\
&\quad | < (l+1)100|l0 > |^2 | < (l+1)1m0|lm > |^2 |Y_{(l+1)m}(\theta',\phi')|^2
\end{aligned}$$

$$+ \quad 2Re\left\{(-i)^{(l-1)-(l+1)}e^{i(\delta_{l-1}-\delta_{l+1})}R_{nlk(l-1)}R_{nlk(l+1)}\frac{4\pi}{3}\left[\frac{(2l-1)}{(2l+1)}\right]^{1/2}\left[\frac{(2l+3)}{(2l+1)}\right]^{1/2}\right.$$
$$< (l-1)100|l0 >< (l-1)1m0|lm >$$
$$\left.< (l+1)100|l0 >< (l+1)1m0|lm > Y_{(l-1)m}(\theta',\phi')Y^*_{(l+1)m}(\theta',\phi')\right\}\Big] \qquad (2.14)$$

Simplifications can first be made by rewriting the Clebsch Gordan coefficients according to the following formulas[8].

$$< (l-1)l(-m)m|10 > \quad = \quad < l1m0|(l-1)m >= \left[\frac{(l-m+1)(l+m+1)}{(2l+1)(l+1)}\right]^{1/2}$$
$$< (l+1)l(-m)m|10 > \quad = \quad < l1m0|(l+1)m >= \left[\frac{(l-m)(l+m)}{(2l+1)l}\right]^{1/2} \qquad (2.15)$$

Substituting the expressions for the Clebsch Gordan coefficients and using the relations[7] to make the summation over m

$$\sum|Y_{lm}|^2 \quad = \quad \frac{2l+1}{4\pi} \qquad (2.16)$$
$$\sum m^2|Y_{lm}|^2 \quad = \quad \frac{l(l+1)(2l+1)}{8\pi}\sin^2\theta \qquad (2.17)$$
$$\cos^2(\theta)|Y_{lm}|^2 \quad = \quad \frac{(l+1)^2-m^2}{(2l+1)(2l+3)}|Y_{(l+1)m}|^2 + \frac{l^2-m^2}{(2l-1)(2l+1)}|Y_{(l-1)m}|^2$$
$$+ \quad 2Re\left\{\sqrt{\frac{((l+1)^2-m^2)(l^2-m^2)}{(2l+1)^2(2l+3)(2l-1)}}Y_{(l+1)m}Y^*_{(l-1)m}\right\} \qquad (2.18)$$

leads to

$$\frac{d\sigma}{d\Omega} \propto \left[R^2_{nlk(l-1)} \frac{6l^2 - l(l+1)\sin^2\theta}{6(2l-1)} + R^2_{nlk(l+1)} \frac{2(l+1)^2 - l(l+1)\sin^2\theta}{6(2l+3)} \right.$$
$$-2Re\left\{ e^{i\delta_{l-1} - i\delta_{l+1}} R_{nlk(l-1)} R_{nlk(l+1)} \right.$$
$$\left. \left. \left(\frac{(2l+1)\cos^2\theta}{6} - \frac{(l+1)^2}{6(2l+3)} + \frac{l(l+1)\sin^2\theta}{6(2l+3)} - \frac{l^2}{2(2l-1)} \right) \right\} \right]$$

This expression can be rewritten in terms of Legendre polynomials according to

$$P_2(\cos\theta) = \frac{1}{2}(3\cos^2\theta - 1)$$

which leads to

$$\frac{d\sigma}{d\Omega} = \frac{1}{4\pi} \underbrace{\frac{4\pi^2 \alpha k_f m\omega}{\hbar} \frac{l R^2_{l-1} + (L+1) R^2_{l+1}}{3(2l+1)}}_{\sigma_{tot}} \cdot$$
$$\left(1 - \underbrace{\frac{l(l-1)R^2_{l-1} + (l+1)(l+2)R^2_{l+1} - 6l(l+1)R_{l+1}R_{l-1}\cos(\delta_{l+1} - \delta_{l-1})}{(2l+1)[lR^2_{l-1} + (l+1)R^2_{l+1}]}}_{\beta} P_2(\cos\theta') \right)$$
$$= \frac{\sigma_{tot}}{4\pi}\left(1 - \beta P_2(\cos\theta')\right)$$

where σ_{tot} is the total cross section for photoionization and β denotes the asymmetry parameter.

Within chosen l orbital it is the radial wave functions - and thus the specific type of atom - that control the appearance of the differential cross section. The σ_{tot} and β factors can be evaluated through for instance Hartree-Fock calculations.

2.3.2 Two photon ionization

With two photons involved, the ionization cross section is even more complex. Especially when the two photons are of different frequency. However the angular part is quite straight forward – in principle just an extra cosine term to the power of four is added – and I will focus on this angular dependence, which is the interesting part in this context, and just collect the different physical constants and the energy and intensity dependence in a constant $C(\omega_1, \omega_2, I)$. Here I is the intensity of the incident radiation and ω_1 and ω_2 the frequencies of the first and second photon in the process.

From second order perturbation theory the differential cross section in the two photon case can, in the dipole approximation, be found to be

$$\frac{d\sigma}{d\Omega} = C(\omega_{is}, \omega_{sf}, I) \left| \underbrace{\sum_s \frac{< f|\vec{\varepsilon}\cdot\vec{r}|s >< s|\vec{\varepsilon}\cdot\vec{r}|i >}{E_i - E_s + \hbar\omega_1 + i\epsilon}}_{M_{fi}} \right|^2$$

where ϵ is a small number which approaches zero and keeps the denominator from giving a singularity. E_i and E_s are the energies of the initial and intermediate states.

Using the wave functions (2.8) and (2.9) and the intermediate wave function

$$\Psi_s = P_{\nu\lambda}(r)Y_{\lambda\mu}(\theta,\phi)$$

together with (2.10) now gives

$$\begin{aligned}
&< f|\vec{\varepsilon}\cdot\vec{r}|s >< s|\vec{\varepsilon}\cdot\vec{r}|i >= \\
&< 4\pi \sum_{L=0}^{\infty} (-i)^L e^{i\delta_L} P_{kL}(r) \sum_{M=-L}^{L} Y_{LM}(\theta,\phi) Y^*_{LM}(\theta',\phi') | \sqrt{\frac{4\pi}{3}} r Y_{10}(\theta,\phi) | P_{\nu\lambda}(r) Y_{\lambda\mu}(\theta,\phi) > \\
&< P_{\nu\lambda}(r) Y_{\lambda\mu}(\theta,\phi) | \sqrt{\frac{4\pi}{3}} r Y_{10}(\theta,\phi) | P_{nl}(r) Y_{lm}(\theta,\phi \cdot > \\
= \quad & \frac{(4\pi)^2}{3} \sum_{L=0}^{\infty} (-i)^L e^{i\delta_L} R_{\lambda l L} < lm|10|\lambda\mu > \sum_{M=L}^{L} < \lambda\mu|10|LM > Y^*_{LM}(\theta',\phi')
\end{aligned}$$

For linearly polarized light the only possibility is again $M = m$. Using this fact and equation (2.11) gives

$$\begin{aligned}
&\sum_s \frac{< f|\vec{\varepsilon}\cdot\vec{r}|s >< s|\vec{\varepsilon}\cdot\vec{r}|i >}{E_i - E_s + \hbar\omega_1 - i\epsilon} = \\
&4\pi \sum_{\lambda L} (-i)^L e^{i\delta_L} \left[\frac{2l+1}{2L+1}\right]^{1/2} < l100|10 >< l1m0|\lambda m > \\
&< \lambda 100|10 >< \lambda 1m0|Lm > Y^*_{Lm}(\theta',\phi') T_{\lambda L}(\omega)
\end{aligned}$$

where $T_{\lambda L}(\omega) = \sum_\nu \frac{<R_{kL}|r|R_{\nu\lambda}><R_{\nu\lambda}|r|R_{nl}>}{E_{nl} - E_{\nu\lambda} + \hbar\omega_{l\lambda} - i\epsilon}$

The selection rule for the L quantum number in the two photon case is $L = l \pm 0, \pm 2$ which leads to four terms in the sum due to the four different possibilities for allowed transitions. These possibilities are $1(l \to l+1 \to l+2)$, $2(l \to l+1 \to l)$, $3(l \to l-1 \to l)$ and $4(l \to l-1 \to l-2)$.

Two of the transitions give the same final state and the differential cross section gets the form

$$\frac{d\sigma}{d\Omega} \propto \sum_m |M_{l+2} + M_l + M_{l-2}|^2$$

Substituting the expressions for the Clebsch Gordan coefficients using (??) and (2.15) gives the following matrix elements:

$$\begin{aligned}
M_{l+2} &= \left(\frac{(l-m+1)(l-m+2)(l+m+1)(l+m+2)}{(2l+1)(2l+3)^2(2l+5)}\right)^{1/2} T_{l+1,l+2} e^{i\delta_{l+2}} Y_{l+2,m}(\theta',\phi') \\
M_{l-2} &= \left(\frac{(l-m)(l-m-1)(l+m)(l+m-1)}{(2l-3)(2l-1)^2(2l+1)}\right)^{1/2} T_{l-1,l-2} e^{i\delta_{l-2}} Y_{l-2,m}(\theta',\phi') \\
M_l &= -\left(\frac{(l-m+1)(l+m+1)}{(2l+1)(2l+3)} T_{l+1,l} + \frac{(l-m)(l+m)}{(2l-1)(2l+1)} T_{l-1,l}\right) e^{i\delta_l} Y_{l,m}(\theta',\phi')
\end{aligned}$$

Apart from equation (2.16), (2.17) and (2.18) the following relations are needed to make the summation over m [[7]]:

$$\sum_m m^4 |Y_{ml}|^2 = \frac{l(l+1)(2l+1)}{8\pi} \sin^2\theta \left(1 + \frac{3}{4}(l-1)(l+2)\sin^2\theta\right)$$

$$2\sum_m (\Lambda^2 - m^2) \left(\frac{l^2-m^2}{(2l+1)(2l-1)}\right)^{1/2} \left(\frac{(l-1)^2-m^2}{(2l-1)(2l-3)}\right)^{1/2} Y^*_{l-2,m} Y_{l,m} =$$

$$\frac{1}{16\pi} \frac{l(l-1)}{2l-1} \left(8\Lambda^2 - 4\left[3\Lambda^2 + (l+1)(l-2)\right]\sin^2\theta + 5(l+1)(l-2)\sin^2\theta\right)$$

$$2\sum_m \left(\frac{(l-1)^2-m^2}{(2l-3)(2l-1)}\right)^{1/2} \left(\frac{l^2-m^2}{(2l-1)(2l+1)}\right)^{1/2} \left(\frac{(l+1)^2-m^2}{(2l+3)(2l+1)}\right)^{1/2} \left(\frac{(l+2)^2-m^2}{(2l+3)(2l+5)}\right)^{1/2}$$

$$Y^*_{l+2,m} Y_{l-2,m} = \frac{1}{16\pi} \frac{(l-1)l(l+1)(l+2)}{(2l-1)(2l+1)(2l+3)} (8 - 40\sin^2\theta + 35\sin^4\theta)$$

I will for simplicity introduce the quantity $X_{pp'}$ which takes care of the radial part and the phase shift

$$X_{pp'} = Re\left(T^*_{\lambda L} T_{\lambda' L'} e^{i(\delta_{L'} - \delta_L)}\right)$$

where p and p' represent the different transition paths ($l \to \lambda \to L$) and ($l \to \lambda' \to L'$) which will be denoted by the numbers for the allowed transition channels established earlier.

Rewriting the sine terms as cosine and gathering all terms of the same power eventually leads to a final expression for the differential cross section in a two photon process

$$\frac{d\sigma}{s\Omega} = C\left(I, \omega_1, \omega_2\right)\left(a + b\cos^2\theta' + c\cos^4\theta'\right)$$

where

$$
\begin{aligned}
a &= \frac{1}{16(2l+1)^2}\left[\frac{(l+1)(l+2)(3l^2+5l+4)}{(2l+1)^2}(X_{11}+X_{22}+2X_{12})\right.\\
&+ \frac{l(l-1)(3l^2+l+2)}{(2l-1)^2}(X_{33}+X_{44}+2X_{34})\\
&+ \left.\frac{6(l-1)l(l+1)(l+2)}{(2l-1)(2l+3)}(X_{13}+X_{14}+X_{23}+X_{24})\right]
\end{aligned}
$$

$$
\begin{aligned}
b &= \frac{1}{8(2l+1)^2}\left[\frac{(l+1)}{(2l+3)^2}\left((l+2)(l+3)(l-4)X_{11}-l(l^2+5l+8)X_{22}-6(l+2)(l^2+l+2)X_{12}\right)\right.\\
&+ \frac{l}{(2l-1)^2}\left((l+1)(l^2-3l+4)X_{33}+(l-1)(l-2)(l+5)X_{44}-6(l-1)(l^2+l+2)X_{34}\right)\\
&+ \left.\frac{2l(l+1)}{(2l-1)(2l+3)}\left((l^2+l+6)X_{23}-3(l-1)(l+4)X_{24}-3(l+2)l-3)X_{13}-15(l-1)(l+2)X_{14}\right)\right]
\end{aligned}
$$

$$
\begin{aligned}
c &= \frac{1}{16(2l+1)^2}\left[\frac{(l+1)(l+2)}{(2l+3)^2}(3(l+3)(l+4)X_{11}-3l(l-1)X_{22}-10l(l+3)X_{12})\right.\\
&+ \frac{l(l-1)}{(2l-1)^2}(3(l+1)(l+2)X_{33}+3(l-2)(l-3)X_{44}-10(l+1)(l-2)X_{34})\\
&+ \left.\frac{2l(l+1)}{(2l-1)(2l+3)}(3(l-1)(l+2)X_{23}-5(l-1)(l-2)X_{24}-5(l+2)(l+3)X_{13}+35(l-1)(l+2)X_{14}\right.
\end{aligned}
$$

This cross section could also be written in terms of Legendre polynomials:

$$\frac{d\sigma}{d\Omega} \propto A + BP_2(cos\theta') + CP_4(cos\theta')$$

2.4 Examples of Angular Distribution

This long derivation has resulted in two simple equations for the differential cross section. It accordingly turns out that, with the exception of ionization of an s orbital where the electron distribution is uniform, it is more probable for electrons to be emitted in some angles than in others. The appearance of this angular distribution depends on many factors which are contained in the asymmetry parameters β, A, B and C. The angular distribution will vary for different electron energies, orbitals, different compounds and different numbers of contributing photons.

When it comes to harmonics there is, as I mentioned in the introduction, both the possibility for one and two photon ionization. Besides the fact that these different processes will give different electron energies they will differ in angular distribution.

An example of this illustrated in figure 2.5 is the ionization of argon with the 15'th harmonic plus an IR photon. The β parameter for the photon energy $16\omega_{IR}$ is approximately -0.3 [6] and corresponding values for A, B and C are 0.2, 0.55 and 0.2 [2].

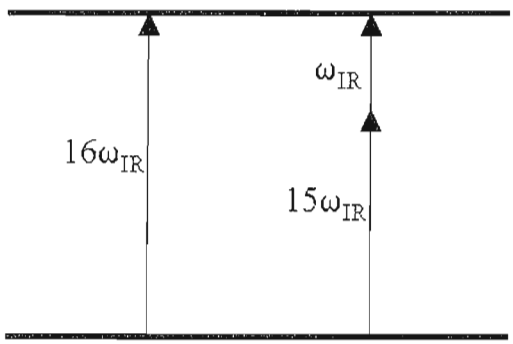

Figure 2.4: Ionization by one or two photons.

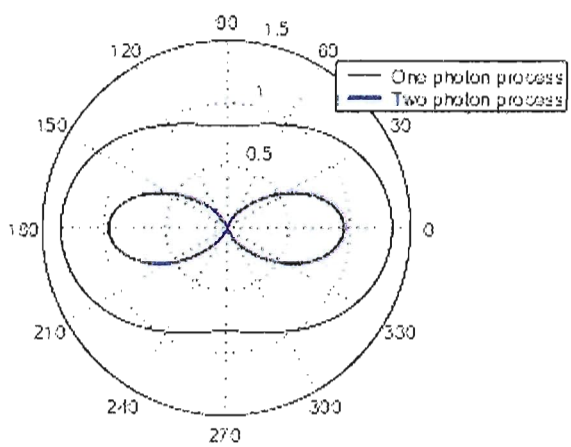

Figure 2.5: Angular distribution for electrons ionized by one or two photons in Argon.

For other values of the asymmetry parameters more complex shapes are produced. Figure 2.6 shows examples of this.

Besides knowledge of the electron energies this angular information can be extracted from one single measurement on an imaging spectrometer.

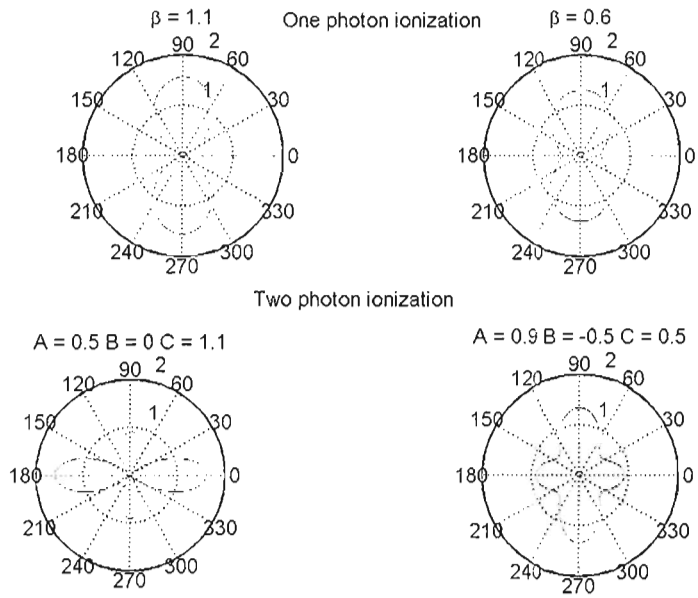

Figure 2.6: Shapes of the angular distribution for different asymmetry parameters.

Chapter 3

Principle of the VMIS

The principle of the VMIS is quite simple. Electrons are created in one end of the spectrometer at the intersection of a gas beam and a laser beam. They are then accelerated by an electrostatic field toward the detector where their position of impact is recorded. From this position information on both energy and angular distribution can be extracted.

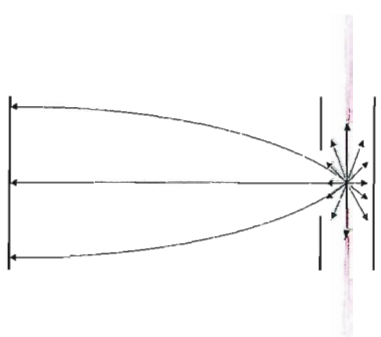

Figure 3.1: Simple sideview of electrode tube with laser and electrons

The image will be a number of concentric circles corresponding to electrons emitted with different energies. The angular distribution of the electrons causes the rings to only be visible in certain angles for which the probability for them to be emitted is large.

3.1 From gas cloud to image

3.1.1 Electrons are emitted

The first step in the velocity map imaging process is the ionization of atoms. A laser is focused in a gas cloud, the atoms in the gas are ionized and electrons are emitted. These electrons will be ejected in certain angles as discussed in chapter 2.

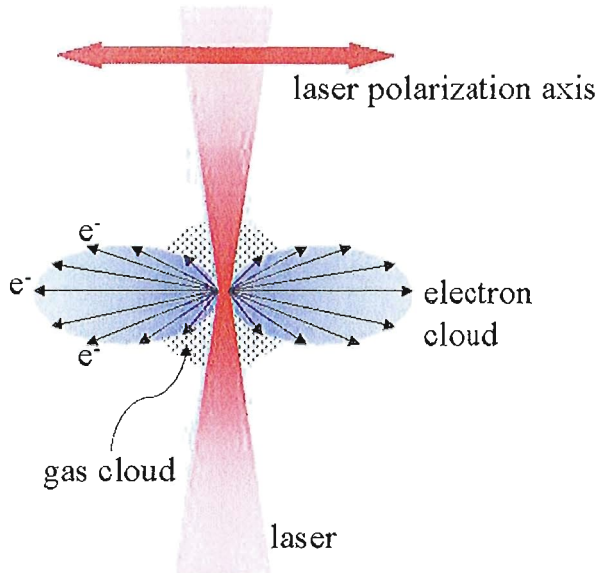

Figure 3.2: A laser ionizes a gas and electrons are emitted

The direction of the electrons depends on what orbital they are emitted from and the energy of the light involved in the photoionization process. If harmonics are used this means that electrons ejected by harmonics of different energy will have different amount of kinetic energy and there will be an angular difference between electrons from the one and two photon processes.

3.1.2 Acceleration towards the detector

In the tube, where the electrons are created, an electrostatic field is introduced. It is a strong positive field that pushes the electrons forward to the detector. This doesn't interfere with the electron ejection angle and it almost doesen't affect their radial velocity at all.

On the way to the detector the electron cloud keeps growing radially and when it hits the MCP an image with cm size concentric circles is produced. Electrons with larger kinetic energy — the ones from higher harmonics — will have a greater radial speed than the ones with lower energy and thus create larger

circles. If the electrons were uniformly emitted in a sphere — as is the case in ionization from an s-orbital — the image would be a complete circle, but because of the angular distributions some angles on the detector will not be hit by an electron at all. The circle will consequently only be visible in other angles. See figure 3.3

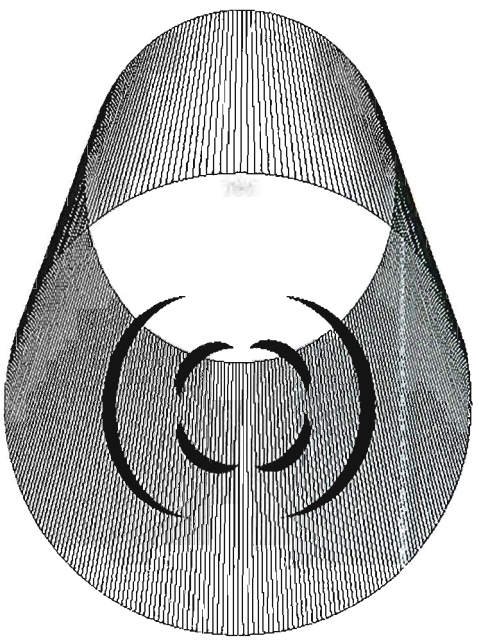

Figure 3.3: Electrons are emitted in the beginning of the electrode tube and an image is produced in the end.

3.1.3 Taking a snapshot

When the electrons hit the front of the MCP they are multiplied and come out as an increased current on the other side and hit a phosphor screen. The phosphor will fluoresce when hit by the current and this produces a visible image. Behind the phosphor is a CCD camera which then takes a picture of the fluorescence.

This is the way images of the photoionization process are produced. Following is a more detailed description of the imaging spectrometer.

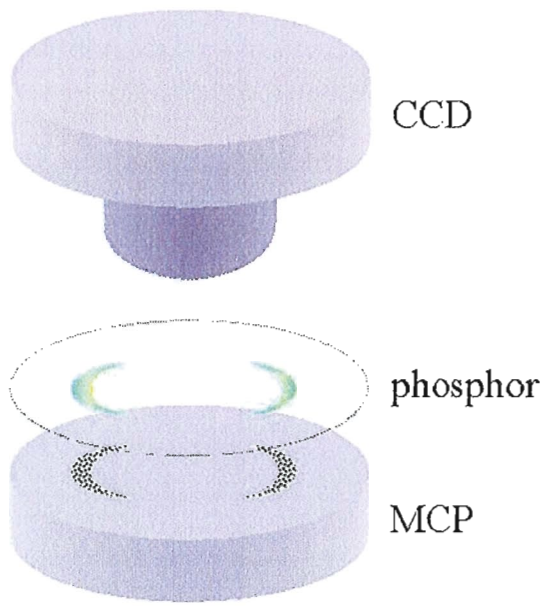

Figure 3.4: The electrons are multiplied by the MCP and the CCD camera takes a picture of the fluorescing phosphor.

3.2 Energy and angle resolved spectra

In contrast to time-of-flight spectroscopy, where information of the electron kinetic energy is given by the time it takes for the particle to reach the detector, velocity map imaging gets the velocity information (kinetic energy and angular distribution) from the two-dimensional image.

The position at which the electron hits the detector is directly proportional to the electrons initial velocity in the yz-direction except for a magnification factor caused by the electric fields component in the yz-direction. This results in a ring on the detector with a certain radius R, related to the expansion speed v_0 of the emitted electron cloud as $R = v_0 t$ where t is the time-of-flight.

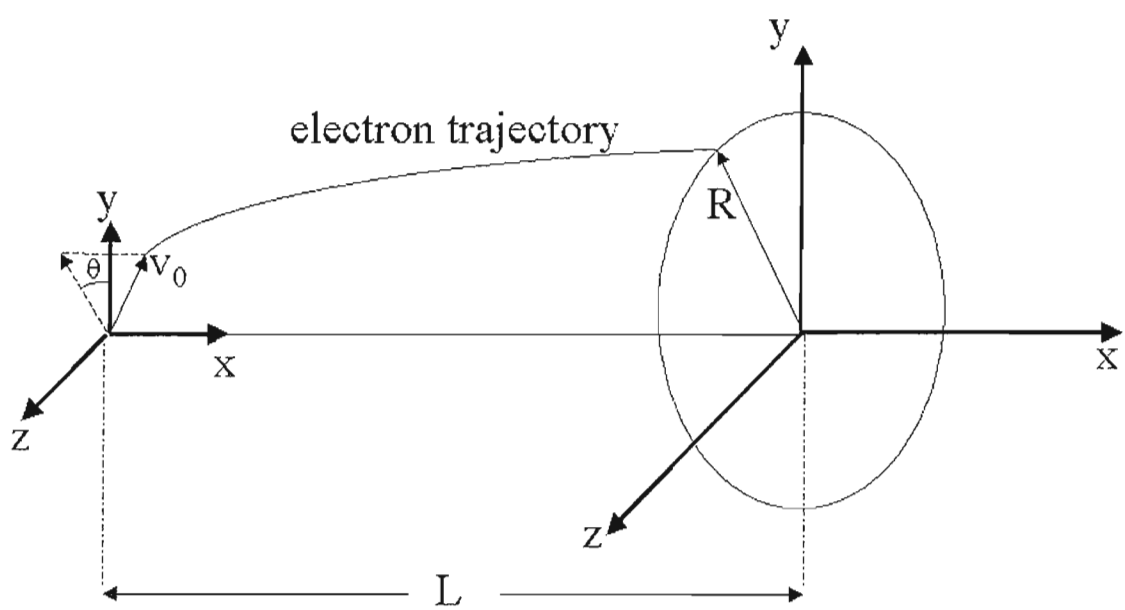

Figure 3.5: Schematic view of the geometry of the imaging.

In the x-direction the electron gets the velocity

$$v_{E,x} = \sqrt{\frac{2T_E}{m}}$$

from the electrostatic field. Here m is the electron mass. The kinetic energy gained by an electron in such a field is

$$T_E = qV$$

where q is the charge of the electron and V is the potential in which it is accelerated. If the electric field component in the yz-direction is disregarded for now and it is assumed that the acceleration region is small compared to the total length L of the spectrometer tube, the time-of-flight can be approximated as

$$t \approx \frac{L}{v_{E,x}} = L\sqrt{\frac{m}{2qV}}$$

This means the radius $R = v_0 t$ will be connected to the initial kinetic energy of the electron according to

$$R \approx L\sqrt{\frac{T_0}{qV}}$$

where $T_0 = mv_0^2/2$.

Figure 3.6: This figure shows the fieldlines which are perpendicular to the electic field.

However the electric field isn't just directed along the x-axis but also slightly radially. It turns out [12] that the component of the field in the yz-direction only contributes with a magnification factor N, that is, the radius of the circles becomes a bit larger than they would with an electric field strictly in the x-direction. The radius of the rings on the image thus behaves as

$$R \approx NL\sqrt{\frac{T_0}{qV}}$$

This magnification factor needs to be determined through calibration for each experimental setup. In this way the energy T_0 of the emitted electrons can be measured from the spectrometer image.

Apart from giving information about the energy of the electrons, the image received from the spectrometer is angular resolved. The angular distribution discussed in chapter 2 causes the rings on the image to be visible only at certain angles. This means that looking at the angular dependent variations on the rings give some knowledge about the emitted electrons. The full three dimensional information can be reconstructed from the projected two dimensional image with a mathematical transformation called Abel inversion which I will discuss later.

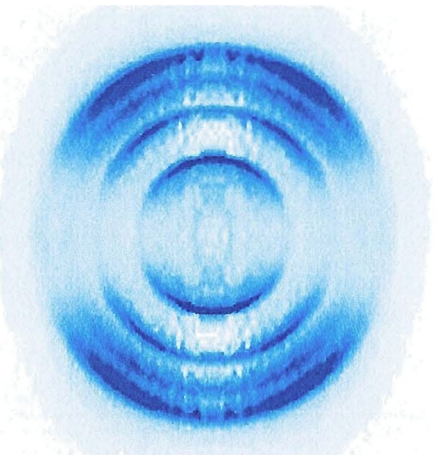

Figure 3.7: An exampel of a real image from an imaging electron spectrometer.

3.3 Focusing the image

The spectrometer consists of a long tube with the detection system in one end. In the other end of the tube is the repeller — a flat circular electrode. A couple of millimeters in front of the repeller is the extractor. a similar electrode but with a hole in the middle. A negative high voltage is applied to the repeller and extractor which creates an electric field in the electrode tube. The electrons are ejected from an area between the repeller and extractor at the crossing of a gas beam and a laser beam.

Ideally one would want the electrons to appear from one single point and from that point be accelerated toward the detector. However there is always a small spatial volume in the gas-laser beam crossing and the electrons are created in this mm large volume. The high positive voltage on the repeller electrode will collapse the electrons in the x-direction (along the TOF axis) into a thin pancake that will propagate toward the detector. Thus it will seem like the electrons are created in this "pancake area".

One of the objectives of the spectrometer is to make all electrons with the same initial velocity — energy and angle — to appear on the same point on the detector regardless of where they were created. By changing the voltage on the extractor, or more specifically changing the ratio between the extractor and repeller voltages $\frac{V_E}{V_R}$, one can focus the electrons so that they all end up on the same point on the focal plane. This is due to the fact that the electrons becomes refracted slightly inwards by the electric field and means that the electrodes serve as electrostatic lenses focusing the image sharply on the detector, compensating for the electrons initial area of creation. The focusing is however only effective when the ionizing happens quite near the center of the ionization region. *SIMION*, the simulation software I have used, shows this effect by picturing the electric high and low potentials as gravitational potentials in the form of hills and valleys (see figure 3.8).

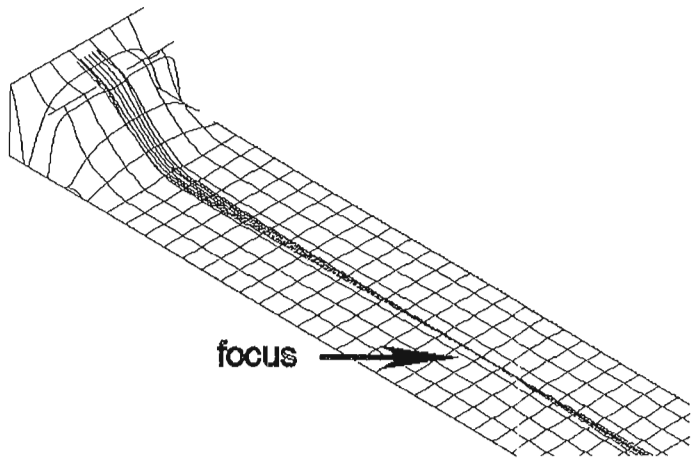

Figure 3.8: An image of the electrode tube with the electric potential pictured as gravitational potential.

Apart from the extractor, extra lenses can be added for fine tuning of the focus and for magnification of the image.

However it is not just focusing the image that is important for a good resolution. Electrons of different energies and angles need to be focused onto different points on the detector. Increasing energy will result in circles with increasing radius on the 2D image. In order to get maximum resolution the radius of the image of electrons with the highest energy has to be as similar to the radius of the detection area as possible. That is, the trajectories for the electrons with maximum energy have to be as widely spread as possible without hitting the walls of the TOF tube. This is achieved by changing the voltage settings on the electrodes for different maximum energies. Higher voltages are needed for higher electron energies.

When the lens configuration is optimal, the resolution of the spectrometer is limited by the detection system.

3.4 Additional operation modes

Besides being an electron imaging machine, the spectrometer can be used for imaging ions. It can also be used in a time-of-flight mode for just measuring the energy of electrons and ions.

3.4.1 Imaging ions

Besides emitted electrons, positive ions are created in the ionization of the gas atoms. Looking at these ions is another interesting application of the spectrometer. Ion spectrometry can also be used for making sure that the received

signal is really from the input gas and not noise like background ionizing. The principle of imaging ions is very similar to imaging electrons. The only difference is that the negative voltages on the repeller and the lenses needs to be switched to positive values. Furthermore the ion imaging is a bit less sensitive to disturbances.

3.4.2 Time-Of-Flight mode

Changing the spectrometer into operating in time-of-flight mode is very easy. An electric circuit that monitors the electron signal is connected to the MCP and the current cased by the electrons or ions is recorded on an oscilloscope. The reason for using the spectrometer this way is that much lower voltages is required for the MCP when you just want to extract the current and not make an image, thereby decreasing the risk of damaging the equipment while aligning the setup. This will be discussed in more detail in section 4.8.

Chapter 4

Design and construction

The design and drawing of the spectrometer chamber is mainly made by Dr. Johan Norin, former PhD student at the Atomic Physics department. I have only made small alterations and additions to it.

In the front of the spectrometer is the detector mount where an MCP is installed. On the flanges near the detector a small vacuum turbo pump and a vacuum gauge is mounted.

The electrode tube is welded on a flange that is held in place between the detector mount unit and the main chamber unit.

On the top of the spectrometer is the gas input, the high voltage vacuum feed troughs for the electrode electric cables, and another vacuum gauge. On the flange on the bottom of the main chamber a large vacuum turbo pump is mounted.

The Laser comes in sideways into the electrode tube trough a small hole. The drawing can be seen in figure 4.1 and 4.2 and a schematic view of the setup is pictured in figure 4.3. Figure 4.4 is a photograph of the final real velocity map-imaging spectrometer.

Following is a more detailed description of the different parts of the imaging setup.

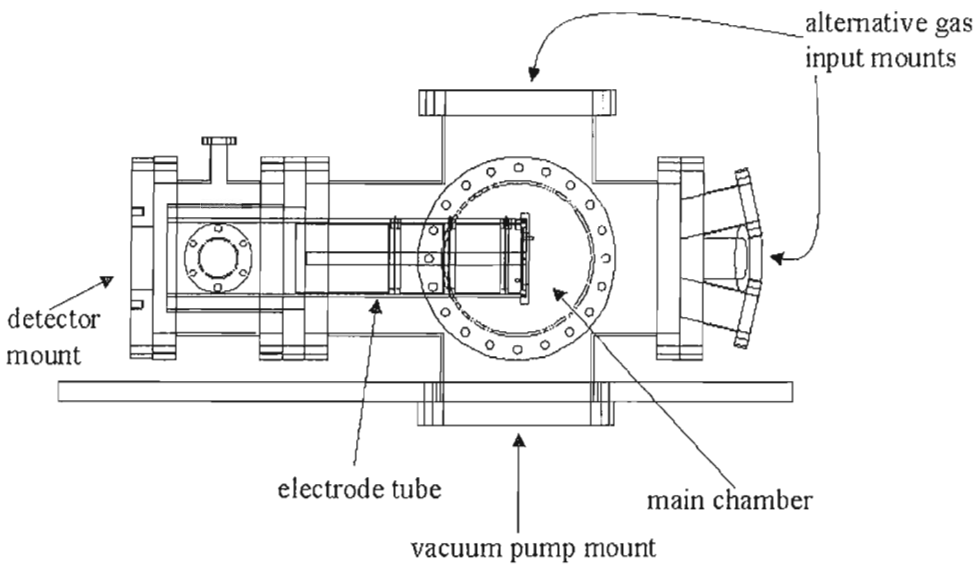

Figure 4.1: Side view drawing of the spectrometer.

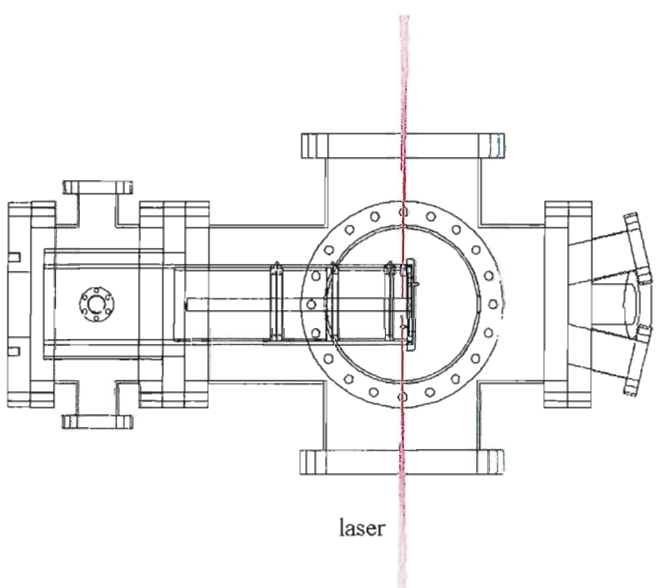

Figure 4.2: Drawing of the spectrometer seen from above. In this picture the position of the laser beam has been illustrated.

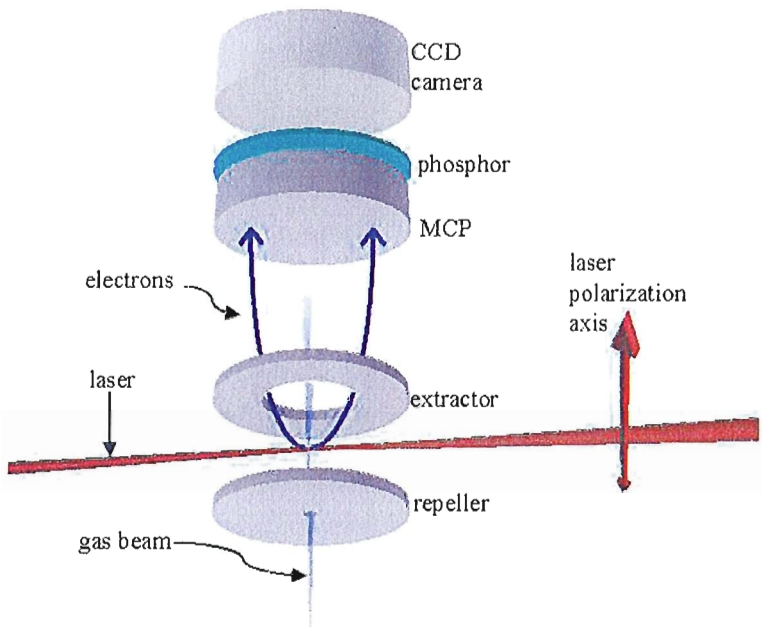

Figure 4.3: Schematic view if the imaging setup.

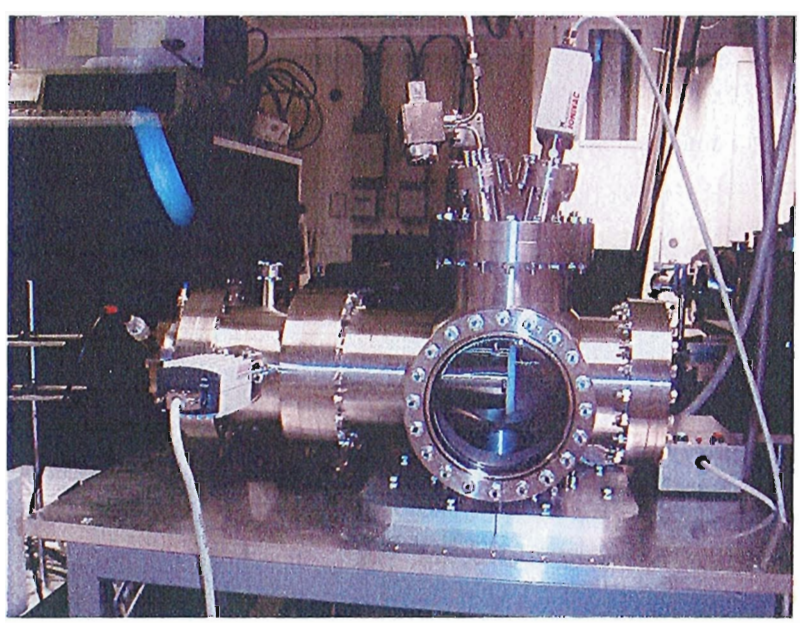

Figure 4.4: Photo of the velocity map imaging spectrometer.

4.1 Electrode design

In order to create the set of electrostatic lenses needed for the imaging I have used a computer program called *SIMION* to simulate the electron trajectories for different lens configurations. Designing and perfecting the electrode dimensions and voltage settings has been one of the most important parts in making this spectrometer.

4.1.1 Desired properties for the spectrometer

In order to get a good measurement the following properties are required:

- Focusing; electrons of the same initial velocity need to be focused onto the same point on the detector. This has to work for wide range of electron energies.
- Spread; the maximum energy electrons have to reach the detector with as large radius as possible.
- Free path; the electrons have to get from the repeller to the detector without smashing into the tube walls or the electrode lenses.
- Linearity; the squared ring radius should vary approximately linearly with the kinetic energy.

To achieve these requirements there are a number of different parameters that can be varied (see figure 4.7)

- Distance between electrostatic lenses, particularly between the point of electron creation and the extractor.
- The number of electrostatic lenses.
- The diameter of the lens openings.
- Voltage settings on the lenses — in particular the extractor/repeller ratio.
- The length of the tube, that is the distance between repeller and detector.

All this has to be taken into account when designing and constructing the velocity map imaging system.

4.1.2 Simulations

The simulation software *SIMION* is constructed for drawing electrodes, setting voltages and calculating trajectories for charged particles in an electrostatic field. It uses potential arrays that define the geometry and potential of electrodes. The potential of the points between the electrodes is determined by solving the Laplace equation. *SIMION* solves this by finite difference methods

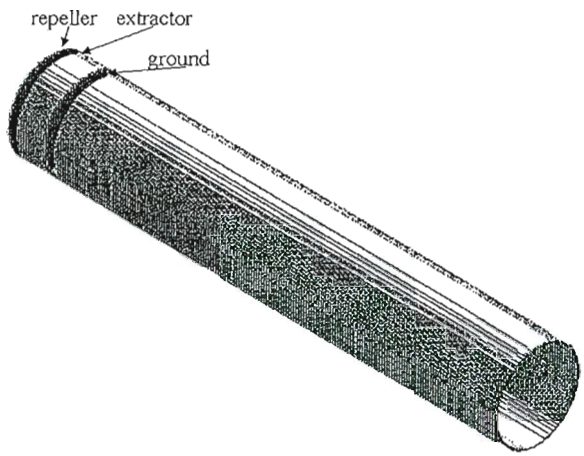

Figure 4.5: The three dimensional view of the electrode tube in SIMION.

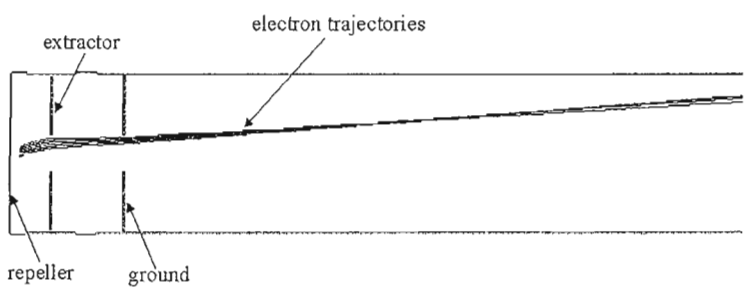

Figure 4.6: Side view of the electrode tube in SIMION with calculated and displayed electron trajectories.

and calls it refining the array. Refined arrays can then be projected as 2D or 3D images into a workbench volume. Here trajectories for ions of different energy, mass and charge can be calculated and displayed.

The electrodes and tube are literally drawn up by hand in *SIMION* and are given specific voltages. They are drawn from side view and by choosing cylindrical symmetry they are rotated around the x-axis. The entire array is then refined, that is the field due to the drawn electrodes is calculated.

Before starting the simulations, mass, energy, angle, charge and start position need to be set for the particles. After this the ion trajectories can be calculated and drawn up. The electrode potentials can then be modified by a fast adjusting system in *SIMION* so that the best voltage settings are achieved.

To start out I chose a lens configuration with repeller (R) extractor (E) and five extra lenses. I soon realized that the last three lenses were unnecessary since they gave the best result when set to 0V. The design of the extra lenses is such that they each consists of circular electrodes with a hole in the middle. Voltage

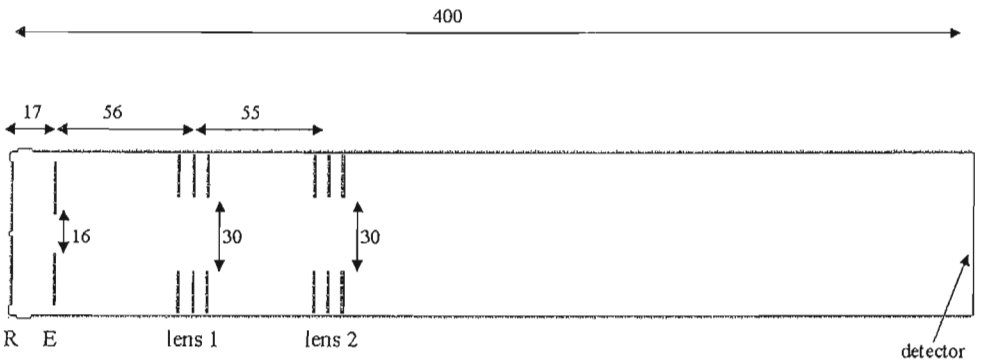

Figure 4.7: This is the final configuration of the electrode tube with repeller, extractor and two extra lenses.

is applied to the electrode in the middle and the two others are grounded. This is the lens construction that gives the best result.

For a specific lens design and length of tube the voltage setting only depend on the maximum electron energy. It is as mentioned earlier the ratio of repeller and extractor voltages that controls the point of focus and this ratio is nearly constant for the different settings.

The final design of electrodes and tube can be seen in picture 4.7.

4.1.3 Voltage settings

The extractor-repeller voltage ratio is about 0.8, but varies slightly for different maximum energies. The spectrometer is made mainly for a maximum electron energy of 20 eV but the voltages are easily changed for lower maximum energies.

Max electron energy	**20 eV**	**10 eV**	**5 eV**
Repeller	-4900 V	-2500 V	-1300 V
Extractor	-4000 V	-2050 V	-1070 V
lens no 1	-2500 V	-1000 V	-400 V
lens no 2	-700 V	-100 V	0 V
V_E/V_R	0.816	0.82	0.823

In practice the focus is never as good as in the simulations and there are very many factors in a real experiment that affect the outcome of the imaging. I have learned that it is sufficient to use only the repeller and extractor since the extra focusing the two lenses provide is often blurred out for various reasons in the actual image. However the extra lenses could still be useful for fine tuning in a very precise measurement, and they are necessary when the image need to be magnified. When the lenses aren't used, the first one of them (closest to the extractor) is set to 0V, in order to make the last bit of the electrode tube field free.

4.2 μmetal shield

Stray magnetic fields — even very small fields — strongly influence electron trajectories and must be directed around the electrode tube. This is accomplished by a magnetic shield of high permeability which guides the magnetic flux around the critical area.

Mu-metal is a nickel-iron alloy (77% Ni, 15% Fe, plus Cu and Mo) which has extremely high magnetic permeability at low field strengths. A shield has been made in this material to fit around and protect the electrode tube.

A hole made in the mu-metal destroys the shielding effectiveness. The penetration from the external field extends internally to a distance approximately equal to the hole diameter. For this reason I have had to keep the holes for electrical cables, laser and gas small.

When μ-metal is altered in some way, like bending, welding or cut, its shielding properties are damaged. After building it, the shield needs to be given a vacuum bake to 1100° to restore the magnetic permeability. After this heating it has to be handled with great care in order to keep its properties.

4.3 Vacuum

A long mean free path is needed for the electrons inside the spectrometer. The number of collisions on the way to the detector has to be as low as possible. This means high vacuum is required in the chamber. Also, the MCP needs high vacuum to not be damaged when high voltage is applied to it. To produce high vacuum the chamber has to be tightly sealed and equipped with a good vacuum pump system.

4.3.1 Vacuum chamber

The chamber is made of stainless steel components with Conflat® flanges. The Conflat® flange is a seal fitting with a knife edge that gets pressed into a copper gasket when screwed on to another flange. This ensures that the chamber is tight enough to contain high vacuum.

4.3.2 Vaccum pumps

Under the main chamber a turbomolecular pump is mounted. It contains rapidly spinning turbine rotors that push gas from the inlet towards the exhaust. The turbopump can not operate if the pressure is too high so before turning it on, the pressure in the chamber needs to be reduced by a for-vacuum pump.

A similar but smaller setup is installed near the detector in order to keep the pressure low there even when gas is let in the main chamber.

Two vacuum-gages are installed on the machine — one on the main chamber and one near the detector. So far the measured vacuum has gone as low as $7 \cdot 10^{-9}$ mbar in the main chamber and $2 \cdot 10^{-8}$ mbar by the detector, but the pressure is still slowly dropping.

4.4 Gas input

The detection gas in the spectrometer is a noble gas and it needs to be present in the ionization region of the spectrometer during an experiment. At the moment a needle valve is installed where small amounts of gas can be let directly in to the main chamber. But in order to get a good result from the imaging the gas-laser crossing has to be quite small and the amount of gas let in to the chamber needs to be as small as possible. This can be accomplished by letting a piezzo electric crystal — triggered by the laser pulses — let small puffs of gas into a tube with a skimmer in one end. The skimmer then gives a very narrow gas beam, and the pulsing of the gas makes sure that as little as possible is let in.

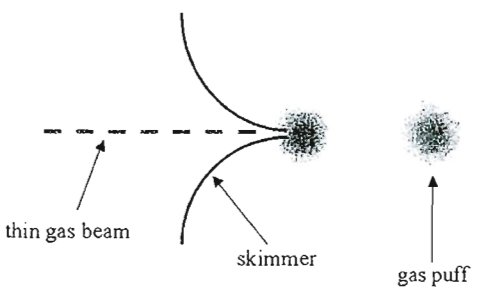

Figure 4.8: Small puffs of noble gas is let in to a tube by a piezzo electric crystal and a skimmer narrows it down to thin gas beam.

4.5 Detection system

The detection system consists of a multichannel plate (MCP) with a phosphor screen on one side and a CCD camera (see figure 3.4).

An MCP is a device which intensifies a signal — in this case electrons — by multiplication of electrons in small channels under the presence of a high electric field. When hit by an electron the channel walls produces more and more secondary electrons. This process amplifies the original signal by several orders of magnitude.

On the back side of the MCP is a layer of phosphor, also supplied with high voltage. The phosphor will fluoresce when hit by an electric current. A CCD camera is then used to make an image of the phosphor screen. The CCD camera transfers the image to a computer where it is saved and later processed.

The detector setup used at the moment is an MCP with a 2.5 cm diameter active area used in a continuous mode. Ideal would be a larger active area and the possibility of using the detector pulsed and trigged by the pulsed laser.

A hit by an electron on the detector gives a very intensive spot which is stronger than spots caused by interference and noise. If the detector is on only in the time frame when electrons hit the MCP surface the weaker noise can be subtracted. In addition to a pulsed MCP a fast CCD camera that takes pictures with a high frequency, and doesn't integrate the image over a long time, is needed.

4.6 Image processing

The image from the CCD camera can be run through a computer program that effectively gets rid of noise. In the program a threshold value can be set and all pixels with intensities above this value is set to one and all others to zero. This sorts out all information in the image not caused by an electron hit and it gives all electron hits the same value to compensate for efficiency fluctuations on the MCP active area. After this processing the images are summed up and the characteristic spectrometer image slowly develops.

Figure 4.9: Processed image from a VMIS.

4.7 Abel inversion

The image from the spectrometer is a two dimensional projection of the three dimensional velocity distribution. If the image contains an axis of symmetry — as is the case in the velocity mapping of electrons — inverse Abel transform can be performed to retrieve the full 3D information.

The Abel transform is an integral transform of the form

$$f(R) = 2\int_{|R|}^{\infty} \frac{g(v)v}{\sqrt{v^2 - R^2}} dv$$

where $f(R)$ represent the 2D radial distribution obtained on the detector.

The Abel inversion that reconstructs the 3D velocity distribution is then

$$g(v) = -\frac{1}{\pi}\int_v^\infty \frac{df(R)}{dR}\frac{1}{\sqrt{v^2 - R^2}}dR$$

The Abel inversion has to be done numerically since there are no analytical functions available in the image, only pixel intensities. Several algorithms have been developed to carry out this procedure [13][14] and for this spectrometer an iterative method, that exploits the close relationship between the 2D projection and the 3D distribution, is used [15].

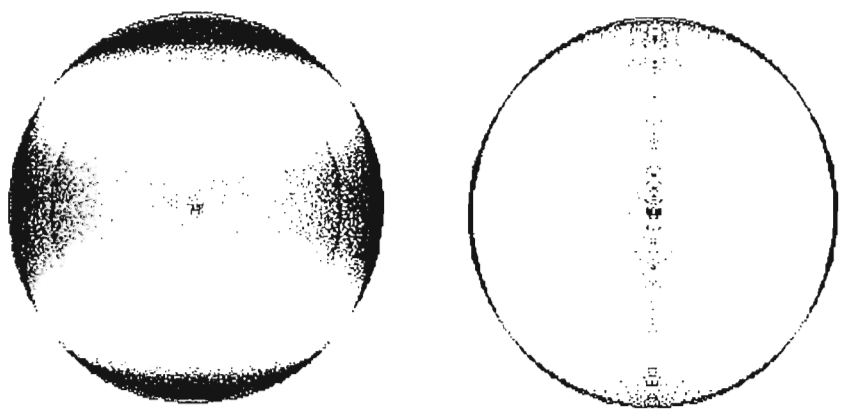

Figure 4.10: To the left is the raw image from the sectrometer and to the right an Abel inversion has been made.

4.8 Time-of-flight mode

A decoupling box with an electric circuit is needed for the spectrometer to be used in TOF mode. It is connected to either the MCP or phosphor screen high voltage inputs and monitor the current produced by the electrons. The circuit can be seen in figure 4.11.

By letting an oscilloscope be trigged by the laser and viewing the current from the decoupling box on the scope screen, the time of flight of the electrons can be measured. This is useful when aligning the laser for an experiment. The MCP needs very high voltages ($\sim 5kV$) to be able to produce an image, but used with lower voltages the current from the electrons can still be monitored on an oscilloscope. The MCP is very sensitive when operated with high voltage and if the laser during the lineup would hit a surface in the spectrometer, a blast of ions would be ejected towards the detector and damage it. This is why it is important to use the spectrometer in TOF mode until the setup is properly aligned. Another reason for using the spectrometer as a TOF is the possibility it gives to separate different compounds in the ionized gas. If the pressure in

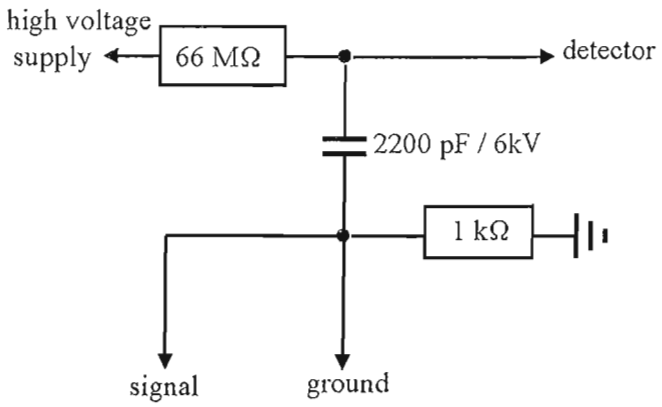

Figure 4.11: Decoupling box to monitor the current caused by the electrons from the MCP.

the chamber is too high, background atoms and molecules can be ionized and measuring the the positive ions time of flight — which is mass dependent — makes it possible to distinguish between the different elements and make sure it is the signal from the detection gas that is being registered.

Chapter 5

Operating the VMIS

5.1 Experiment at AMOLF

During the course of my diploma work I went for a week to the AMOLF institute in Amsterdam and participated in some measurements with a similar spectrometer. The aim was to see a real velocity-mapping setup in action and get some practical experience of the different elements of an imaging experiment. The visit was very rewarding and some of the components in the setup have been inspired from the imaging machine I saw at AMOLF.

5.1.1 Experiment

The purpose of the experiment was to examine the DNA component Uracil and the defragmentation process that occurs under the influence of a laser. The Uracil was a white powder that was heated in a oven and entered into the ionization region trough a small hole. The setup of the spectrometer was very similar to mine except for the gas input. Both a mode locked Nd:YAG laser and a femtosecond laser were used in the test. One of the major difficulties was to get the laser perfectly aligned in the middle of the electrode tube, where it coincided with the gas beam.

The signal from the ions was first viewed with the spectrometer in time-of-flight mode on an oscilloscope and then imaged and computer processed.

5.1.2 Result

During my week in Amsterdam, unfortunately, no signal was acquired from the uracil. However the signal from the background ionization was quite strong and I was able to make an image of this. The conditions for imaging background ions where not perfect for a sharp image since the ions come from a rather large volume where the laser is strong enough to ionize. I did get a nice image though

where it can be seen that the photo dissociation has an angular distribution (see figure 5.1).

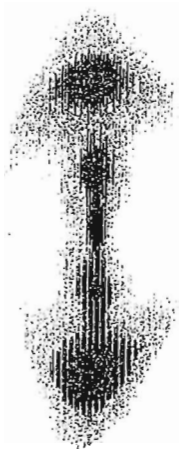

Figure 5.1: Result from imaging a background ion on an imaging machine at AMOLF, Amsterdam.

The week after I left AMOLF I learned that the experiment was now working and that a good signal was received from the Uracil.

5.2 Operation of the spectrometer

Here follows a short description on how to operate the VMIS and the first steps in making an experiment.

5.2.1 Vacuum

In addition to the need for high vacuum in the spectrometer when an experiment is being conducted, vacuum is required when an experiment is not running in order to keep the inside of the chamber from being contaminated and for the MCP which need vacuum even when it is just stored.

To start the vacuum pumps:

- Make sure the vents between turbo pumps and fore-vacuum pumps are closed, and that cooling water is on.
- Start both for-vacuum pumps, wait a couple of seconds and then open the vents.
- When the pressure has gone down below $1 \cdot 10^{-1}$ mbar, both turbo pumps can be turned on.

5.2.2 MCP, phosphor and CCD camera

- Two high voltage supplies are needed for the MCP and phosphor. It is important to have some sort of safety switch connected to these power supplies that shuts the power off if it goes above a certain limit value. This is used to protect the sensitive MCP and phosphor. The voltages have to be raised very slowly if it is the first time in long they are being used. The total process takes a couple of hours and is done according to a scheme in the MCP manual.
- When the MCP is used frequently the voltages can be switched on much faster. The voltage settings for the MCP and phosphor screen for different usage are listed in the manual.
- The CCD is turned on. Make sure the cable for cooling the camera is inserted properly, the camera has to be cooled at all times when it is on.

5.2.3 Laser alignment

When a narrow gas input exists it is important that the laser beam is very well centered in the ionization region so that the focus of the laser overlaps with the gas beam. Otherwise there will be no signal at all. Within the region of gas-laser-overlap where a signal can be detected, changing the laser alignment slightly can improve the focus of the electrons.

5.2.4 Repellor and extractor voltages

The repeller and extractor need one high voltage supply each and if the extra lenses are used, one supply for each of them is needed to. It is important that these power supplies are very precise because the voltages don't have to be off by much for the focus to change a lot.

After the laser alignment is optimized, the voltages on the repeller and extractor can be modified until the best possible resolution is achieved.

5.3 Planned test

For testing the spectrometer I have been planning a small experiment where background atoms are ionized. When the pressure in the chamber is $\sim 7 \cdot 10^{-7}$ mbar there is enough air in the ionization region to be able to see a signal from ionized air particles. The idea is to measure ions since this is much easier than measuring electrons, no μ-metalshield is necessary for instance.

A femtosecond laser beam from the kHz system in the next room has been aligned through the spectrometer. The needle valve is used to carefully let some air into the chamber to raise the pressure a bit since the current vacuum is too high to see any ions from the background right now.

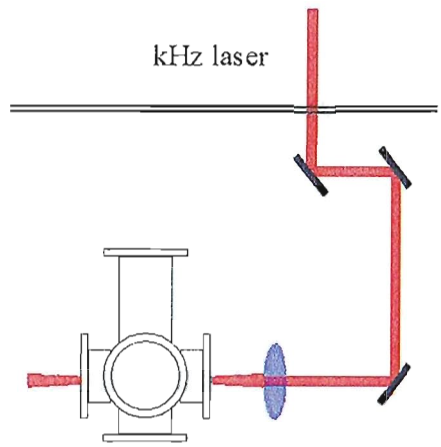

Figure 5.2: A femtosecond laser is aligned trough the spectrometer to be used in a background ionizing experiment.

The TOF signal would first be monitored on an oscilloscope and after making sure the laser alignment is good an image of the ions would be made.

Chapter 6

Summary and outlook

6.1 Summary and Outlook

This diploma work has consisted of designing and constructing a velocity-map imaging spectrometer.

I started out by doing simulations of electron trajectories in an electric field which led to the design of the electrode tube with repeller, extractor and the extra electrostatic lenses. The voltage settings on the electrodes — which give the important result of focusing the electron trajectories — were also decided from the simulations.

Next, all parts needed for the spectrometer were ordered and the job of building the chamber started, including designing a table, tightening screws and installing the vacuum system. Apart from the chamber, many other components were needed, such as an MCP-phosphor detector, a CCD camera, high power supplies, TOF circuit and and vacuum valves, which were ordered, collected and tested.

The final result is now standing in the pico lab in the Atomic Physics department ready to be tested.

The first experiment planned for the spectrometer is a test where elements from the background air will be ionized and the positive ions imaged. The next step for the spectrometer is to start imaging electrons and to optimize laser alignment and electrode voltages to get a good and stable setup. A pulsed detector, a fast CCD camera and a gas input with the possibility to make a narrow atom beam are other things that need to be investigated.

In the future, the imaging spectrometer will be used for characterizing attosecond pulses, especially when pulse trains become so short that electron energy distributions from consecutive harmonics and side bands overlap and angular resolution is necessary for the analysis. Furthermore the imaging machine will be a good tool for doing atomic physics in general and for examining energy and angular distributions of electrons and ions.

Acknowlegements

I want to thank my supervisor Prof. Anne L'Huillier for giving me the opportunity to have this exiting project as a diploma work and for all her help, advise and inspiration.

A special thanks goes to Dr. Johan Norin and Dr. Allan Johansson for all their work with the spectrometer, their help and inspiring collaboration.

Thank you to Prof. Marc Vrakking for advice and for letting me come to AMOLF and participate in an experiment, and a special thanks to Dr. Franck Lepine for making my week at AMOLF so useful and inspiring.

Thanks to my mother for constant support and cheer leading and thank you Ola Synnergren for support, advise and help.

So many people have contributed to the spectrometer along the way and I want to give a special thanks to you all for your time and effort.

Bibliography

[1] A.T.J.B. Eppink and D.H. Parker, Rev. Sci. Instrum. **68** (9), 3477 (1997)

[2] S.A. Aseyev, Y. Ni, L.J. Frasinski, and M.J.J. Vrakking, Phys. Rev. Lett. **91** (22), 223902 (2003)

[3] A. L'Huillier and F. Krausz, High-order harmonic generation and its application to attosecond metrology.

[4] Brandsen and Joachain, Physics of Atoms and Molecules, Second Edition

[5] Gunnar Ohlén, Quantum Mechanics II

[6] D. J. Kennedy and S. T. Manson, Photoionization of the Nobel gases, Physical Review A 5 (1971)

[7] E. Arnous, S. Klarsfeld and S. Wane, Angular Distribution in the Two-Quantum Atomic Photoeffect, Physical Review A 7 (1972)

[8] I. Lindgren J.Morrison, Atomic Many-Body Theory, Second Edition

[9] H. K. Tseng, R. H. Pratt, S. Yu and A. Ron, Photoelectron angular distributions, Physical Review A 17 (1977)

[10] J. W. Cooper, Photoelectron-angular-distribution parameters for rare-gas subshells, Physical Review A 47 (1992)

[11] P. M. Paul, Thése de doctorat (2001)

[12] F. Rosca-Pruna, PhD Thesis (2001)

[13] C. Bordas, F. Paulig, H. Helm, and D. L. Huestis, Rev. Sci. Instrum. **67**, 2257 (1996)

[14] J. Winterhalter, D. Maier, J. Honerkamp, V. Schyja, and H. Helm, J. Chem. Phys. **110**, 11187 (1999)

[15] M.J.J. Vrakking, Rev. Sci. Instrum. **72**(11) 4084(2001)